Contrib Mineral Petrol (2015) 169:25
DOI 10.1007/s00410-015-1114-y

ORIGINAL PAPER

Rare earth element evolution and migration in plagiogranites: a record preserved in epidote and allanite of the Troodos ophiolite

Michael Anenburg · Yaron Katzir · Dieter Rhede · Niels Jöns · Wolfgang Bach

Received: 1 October 2014 / Accepted: 14 January 2015

Abstract Plagiogranites from the Troodos ophiolite in Cyprus are occasionally epidotised, either partially or completely. Epidotisation phenomena include replacement of pre-existing minerals and filling of miarolitic cavities. In addition to epidote, miarolites in one plagiogranite body (located near the village of Spilia) contain coexisting ferriallanite-(Ce) and allanite-(Y). Textural and geochemical evidence indicates that late-stage REE-enriched granitic melt facilitated crystallisation of magmatic ferriallanite-(Ce). High REE contents persisted after fluid exsolution, causing crystallisation of allanite-(Y) from hydrothermal fluids in the miarolites. The REE pattern of the hydrothermal allanite-(Y) is characterised by LREE and Eu depletion, similar to the parent plagiogranitic magma. As allanite had sequestered most of the REE in the fluid, epidote took over as the principle hydrothermal mineral. Epidote in Troodos plagiogranites records a fluid evolutionary trend beginning with REE-rich–Eu-depleted similar to allanite-(Y) and gradually transforming into the REE-depleted–Eu-enriched pattern prevalent throughout 'conventional' sub-seafloor fluids. A comparison of allanite-bearing and allanite-absent plagiogranites from the same locality suggests that REE-bearing fluids migrated from the plagiogranites. Similar fluid evolution trends observed in diabase-hosted epidote, located adjacent to a large plagiogranite body, suggest influx of plagiogranite-derived REE-bearing fluids. Epidotisation in oceanic settings is usually considered to be the result of alteration by high fluxes of seawater-derived hydrothermal fluids. Although epidotisation by magmatic fluids has been suggested to occur in plagiogranites, our study shows that this autometasomatic process is the dominant mechanism by which epidosites form in plagiogranites. Furthermore, epidotisation of diabase has been attributed solely to seawater-derived fluids, but we show that it is possible for diabase-hosted epidosites to form by migration of plagiogranite-derived fluids.

Keywords Allanite · Troodos · Plagiogranite · Ophiolite · Epidotisation

Electronic supplementary material The online version of this article (doi:10.1007/s00410-015-1114-y) contains supplementary material, which is available to authorized users.

Communicated by Timothy L. Grove.

M. Anenburg (✉) · Y. Katzir
Geological and Environmental Sciences, Ben-Gurion University of the Negev, Beersheba 84105, Israel
e-mail: michaela@post.bgu.ac.il

Y. Katzir
e-mail: ykatzir@bgu.ac.il

Present Address:
M. Anenburg
Research School of Earth Sciences, Australian National University, Canberra 0200, Australia

D. Rhede
Deutsches GeoForschungsZentrum, Potsdam 14473, Germany

N. Jöns · W. Bach
Fachbereich Geowissenschaften, Universität Bremen, Bremen 28359, Germany

Present Address:
N. Jöns
Department of Geology, Mineralogy and Geophysics, Ruhr-Universität Bochum, Bochum 44801, Germany

Introduction

The origin of plagiogranites in present day mid-oceanic ridges and in ophiolites has been intensely debated in recent

Published online: 17 February 2015

years using field-based and experimental petrological studies assisted by geochemical and isotope evidence (Koepke et al. 2004, 2007; Brophy 2009; Rollinson 2009; France et al. 2010; Grimes et al. 2011; Brophy and Pu 2012; Freund et al. 2014). Measured rare earth element (REE) contents and patterns of rocks and minerals are routinely used in model calculations to constrain the source rocks of plagiogranitic magmas and their formation process (e.g. Gerlach et al. 1981; Pedersen and Malpas 1984; Flagler and Spray 1991; Borsi et al. 1996; Twining 1996; Floyd et al. 1998; Luchitskaya et al. 2005; Rudnev et al. 2005; Dilek and Thy 2006; Rollinson 2009; Brophy 2009; Brophy and Pu 2012; Freund et al. 2014). Important hosts of REE in plagiogranites are the epidote group minerals. Allanite, a REE-rich epidote group mineral, is common in continental granites (Frei et al. 2004; Gieré and Sorensen 2004; Armbruster et al. 2006), but its occurrence in plagiogranites of ophiolites and modern oceanic crust has been sparsely reported and has yet to be properly discussed (Mason 1981; Flagler and Spray 1991; Kaur and Mehta 2005; Castelli and Lombardo 2007; Nakamura et al. 2007; Silantyev et al. 2010; Rollinson 2014). For example, Flagler and Spray (1991) used mineral/melt partition coefficients (*D*) to differentiate several models of plagiogranite generation. However, they did not include allanite (a significant REE reservoir) in their models, even though it exists in their plagiogranite. More recently, Brophy and Pu (2012) did use allanite in their model, but they assumed that allanite was of magmatic origin. This may not be accurate, as allanite can possibly be of hydrothermal origin, thus affecting the appropriate REE partition coefficients to be used (Gieré and Sorensen 2004; Frei et al. 2004). Allanite has also been shown to be a fractionating phase in formation of some plagiogranites (Koepke and Seidel 2004; Montanini et al. 2006), stressing the importance of understanding their role in plagiogranite genesis. Allanites are commonly texturally and temporally transitional to epidotes, and the occurrence of allanite has to be studied in the wider context of hydrothermal activity and epidotisation in plagiogranites.

Allanite has been observed in plagiogranites of the Troodos ophiolite in Cyprus (Wilson 1959; Chutas 1997), where it occurs as closely associated allanite-(Y) and ferriallanite-(Ce), concentrated in epidote masses. This work studies the textural and geochemical properties of both allanite types and their relation to epidote, and explores the epidotisation process of oceanic plagiogranites in particular and of ophiolites in general.

Geological setting and sampling

The Troodos ophiolite is located on the island of Cyprus in the easternmost Mediterranean (Fig. 1). It comprises a well-ordered and mostly non-deformed Penrose-type sequence of mantle ultramafic rocks, crustal gabbro, sheeted dykes (also known as diabase), and pillow lava basalts overlain by deep sea sediments. Plagiogranites commonly occur near the gabbro–diabase contact, but rarely also fully included within the gabbro and diabase units, farther away from the contact.

Samples were collected from plagiogranite bodies located to the east of the main ultramafic complex. An additional sample of an epidotised diabase from the base of the sheeted dyke complex was collected to the west of the main ultramafic complex, near Lemithou. The sample localities are named after nearby villages (Fig. 1; Table 1).

Petrography

The primary mineral assemblage of the plagiogranites in this study is quartz + plagioclase ± amphibole ± pyroxene. Accessory minerals include zircon, titanite, and magnetite. Most plagiogranites have experienced post-magmatic alteration represented by minerals such as pumpellyite, hydrothermal amphiboles, micas, chlorite, and sericite. However, the most conspicuous post-magmatic minerals are the epidote group minerals: epidote and allanite, which are the focus of this study.

On a hand specimen scale, plagiogranites can be unepidotised (Fig. 2a), partly epidotised (Fig. 2b), or completely epidotised (Fig. 2c). Epidotisation can occur across several centimetres as seen in the unepidotised dark grey part and epidotised light green part of the rock in Fig. 2d, e, or as veins in otherwise unepidotised plagiogranites (Fig. 2f).

Epidote

Texturally, epidotisation of plagiogranites occurs in two different types. The first is the 'miarolite' type: filling of miarolitic cavities with epidote. The most impressive examples of miarolitic epidotes occur in the Spilia plagiogranite (Fig. 3). In some cases, the miarolites are extremely small, giving the epidote an interstitial character rather than a miarolite-filling appearance, common in samples collected from Polystipos and Platanistasa (e.g. the high-relief epidote in the middle of Fig. 4a). In many cases though, miarolitic epidote appears as euhedral or splaying aggregates of crystals (Figs. 3a, b, 4b, g). The crystals are commonly zoned, but no consistent type of zoning is observed. The most common type of zoning is normal zoning (with high-Δ cores and low-Δ rims, e.g. Fig. 4c). However, reverse or oscillatory (Fig. 4d) zoning are also present. The miarolites are occasionally lined with euhedral hexagonal quartz (top left of Fig. 4e, left of Fig. 4g, and bottom of Fig. 4h), amphiboles (middle

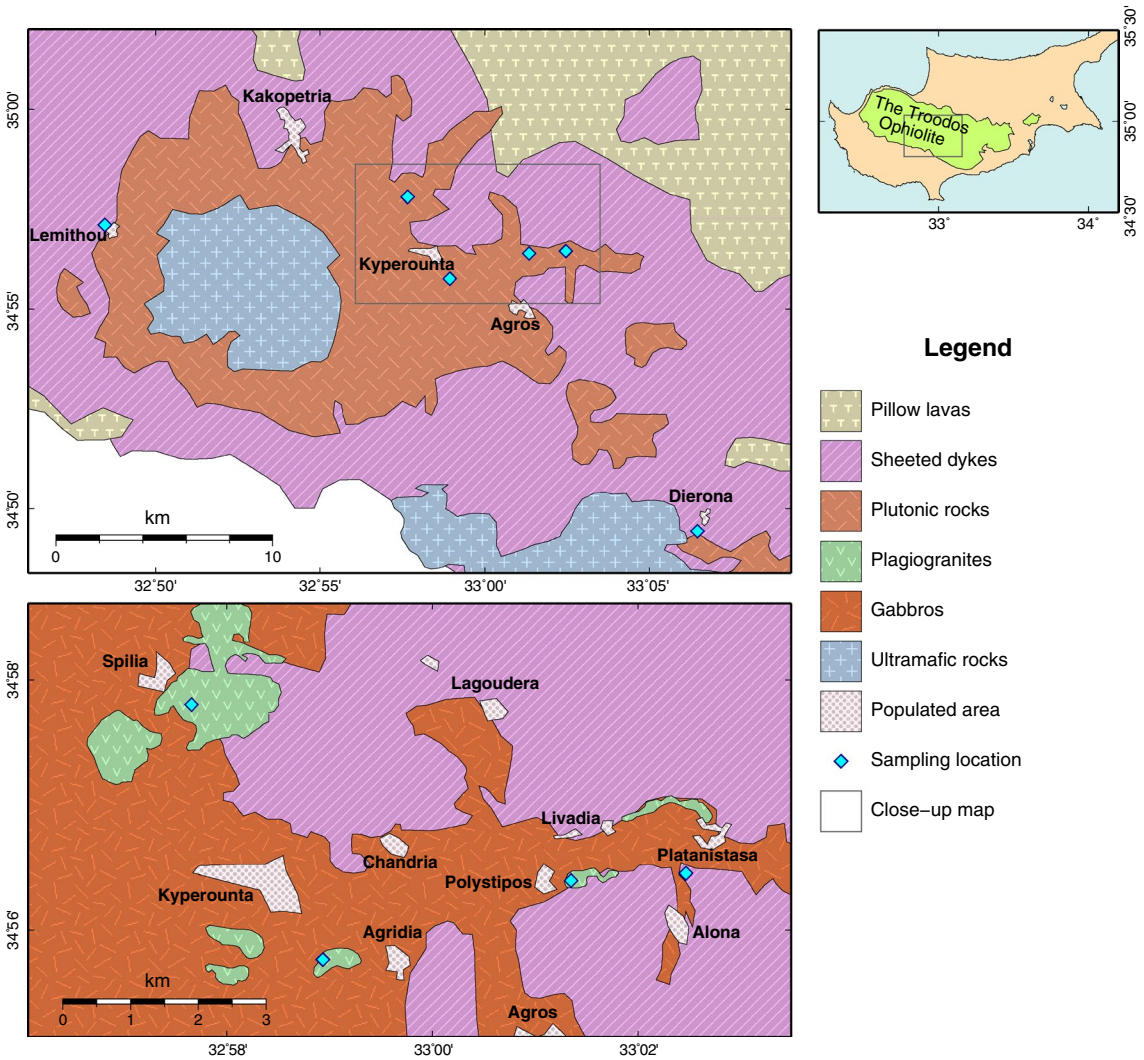

Fig. 1 Simplified geological maps showing the major rock types in the Troodos ophiolite and the sampling locations. Top map based on Constantinou (1995); bottom map based on Malpas (1987)

of Fig. 4h), and magnetite (Fig. 4f) that seem to predate epidote, while chlorite (top right of Fig. 4c) or calcite (middle left of Fig. 4g, intermediate grey) occasionally fill remaining cavities after epidote growth. Miarolitic epidote also fills in cavities inside plagioclase, suggesting growth after plagioclase dissolution rather than a dissolution–precipitation process (Fig. 4d, i). Euhedral plagioclase that lined miarolitic cavities is mostly replaced by epidote, leaving only ghosts of relic crystals (e.g. Fig. 4d, e). Note that epidotisation of plagioclase is strongest adjacent to the miarolitic epidote but much weaker less than a millimetre away (e.g. Fig. 4d).

The second textural type of epidote is the 'replacement' type: epidote is anhedral and commonly appears to replace other minerals (Fig. 5a–c). Replacive epidote is often porous and characterised by patchy and irregular zoning. This textural type also dominates epidosites: quartz + epidote rocks (as defined by Flawn 1951), from the sheeted dyke complex (Fig. 5d). The 'replacement' type occasionally occurs in association with brittle fractures in plagiogranites (e.g. Fig. 5c) or as veins of epidosite—in the sense of quartz + epidote rock—inside otherwise unaltered plagiogranites (the top–bottom trending vein in Fig. 5e).

The two textural types described here only represent the two most common 'end members' of epidote observed in the rocks. In many cases, epidote cannot be classified on textural grounds. It is very common to see miarolitic epidote overprinted by 'replacement' epidote. For example, the bright, weakly zoned, epidote (likely of 'miarolite' type) in the top left of Fig. 5f resides in the core region of a larger, darker, 'replacement' epidote that fills most of the image area. In all cases where the two types coexist and timing can be determined, the 'replacement' epidote postdates the 'miarolite' epidote.

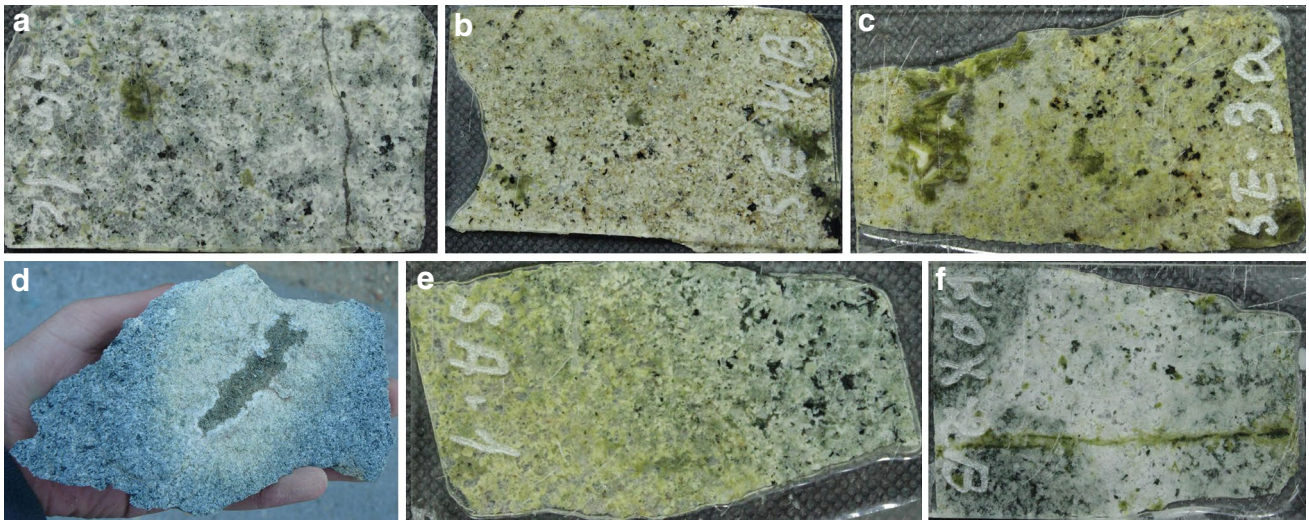

Fig. 2 Polished sections of samples **a** SG-1C: unepidotised plagiogranite, **b** SE-4B: slightly epidotised plagiogranite, **c** SE-3A: epidotised plagiogranite, **d** epidote-filled miarolite encircled by epidosite halo, **e** SA-1: gradual transition from plagiogranite (*right*) to epidosite (*left*), and **f** KPX-2B: epidosite vein cross-cutting a leucoplagiogranite containing melano-plagiogranite enclaves

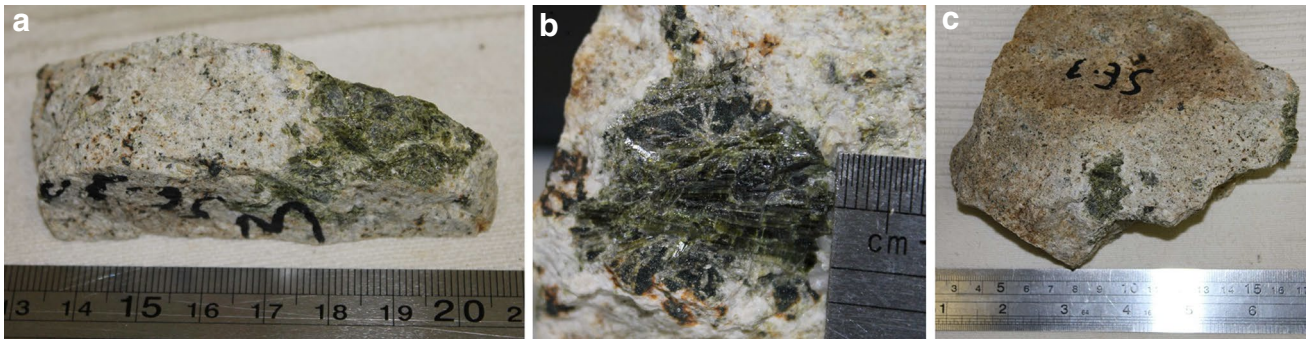

Fig. 3 Photographs of samples **a** SE-3A, **b** SE-2 and **c** SE-1, showing epidote-filled miarolites

Allanite

Allanites in the Troodos plagiogranites can be divided into two different mineral species: allanite-(Y) and ferriallanite-(Ce), based on the more dominant rare earth element and iron contents (see below). The first type, allanite-(Y), was observed only in Spilia. It occurs as oscillatory zoned allanite–epidote with the cores containing more allanite zones than epidote and the rims contain more epidote (Fig. 6a, b). This type of allanite resides in the interiors of miarolitic epidote masses (similar to Pin et al. 2006), and it has a dark red pleochroic colour with no anomalous birefringence colours. In some cases, signs of late alteration and recrystallisation can be seen in this type (Fig. 6b). The second type, ferriallanite-(Ce), was observed both in Spilia and in Kyperounta. Instead of allanite–epidote zoning, it is composed of one single grain with sharp borders against the epidote in which it is located. The backscattered electron image shows that it has neither oscillatory nor patchy irregular zoning (Fig. 6c; however, it does feature consistent chemical zoning, see below). Ferriallanite-(Ce) has pale greenish-brown pleochroic colour with similar anomalous interference colours.

Analytical methods

LA-ICP-MS

Trace element contents of epidote were measured in situ by LA-ICP-MS (laser ablation—induced coupled plasma—mass spectrometry) using a NewWave UP193 solid-state laser coupled with a Thermo Finnigan Element2 mass spectrometer at the Department of Geosciences, University of Bremen, Germany. Standards and samples were ablated with an irradiance of ca. 1 GWs^{-2} and a pulse rate of 5 Hz.

Table 1 List of samples used in this study

Locality	Easting	Northing	Sample	Epidote-group minerals
Lemithou	482433	3867720	Cy4-1-10	ep
Kyperounta	498381	3865211	KPC-2X	ep
			KPG-1	ep + ep–aln-(Ce)
			KPX-2B	ep
Platanistasa	503754	3866488	H-3B	ep
			PAB-2A	ep
			PAI-4A	ep
Polystipos	502055	3866380	PXD-1A	ep
			PXD-2B	ep
Spilia	496436	3868984	SE-3A	ep + aln-(Y)
			SE-4B	ep
			SG-1B	ep + aln-(Y) + faln-(Ce)
			ST-4	ep
			SA-1	ep + aln-(Y)?

Coordinates in UTM zone 36 S. Mineral abbreviations: ep: epidote, ep–aln-(Ce): REE-poor allanite-(Ce), aln-(Y): allanite-(Y), faln-(Ce): ferriallanite-(Ce)

Spot size for standards was 75 μm and line scan speed of 4 μm s^{-1}. Most samples were ablated using a 100 μm spot size, and several others were ablated using a 75 μm spot size. Spot size of 50 μm was used only for a small fraction of the samples. Several samples were analysed using the line mode with settings similar to the standards. A pre-ablation run was carried out to clean the surface. We used helium (0.73 l min^{-1}) as sample gas and added argon (0.9 l min^{-1}) as make-up gas; plasma power was 1,200 W. The following isotopes were analysed: ^{29}Si, ^{43}Ca, ^{47}Ti, ^{51}V, ^{53}Cr, ^{59}Co, ^{63}Cu, ^{66}Zn, ^{88}Sr, ^{89}Y, ^{90}Zr, ^{139}La, ^{140}Ce, ^{141}Pr, ^{146}Nd, ^{147}Sm, ^{151}Eu, ^{158}Gd, ^{159}Tb, ^{161}Dy, ^{165}Ho, ^{166}Er, ^{169}Tm, ^{172}Yb and ^{175}Lu. All isotopes were analysed at low resolution with five samples in a 20 % mass window and a total dwell time of 25 ms per isotope. Blanks were measured during 20 s prior to ablation. For external calibration, we measured the NIST612 standard reference material (SRM), a sodium silicate glass, after each 8–12 analyses (standard bracketing). Calcium was used as internal standard with an assumed concentration of 16.66 wt% for most analyses. Ca contents measured by EMPA were used for REE-rich epidotes where the 16.66 % assumption was not accurate. For data quantification, we used the Cetac GeoPro software with the concentrations for NIST612 given in Jochum et al. (2011). Data quality was assessed by repeated analyses of BCR2G and BHVO2G basaltic glasses (from United States Geological Survey) over the analytical session. The relative standard deviation (RSD) of these two glasses is used as an indicator of precision. Overall precision was better than 10 % for all elements. A summary for each element is given in Table 2, including accuracy with respect to the reference values after Jochum et al. (2005).

EMPA

Epidote chemical analyses were performed using a JEOL Superprobe JXA-8900R EMPA (electron microprobe analyser) at the Department of Geosciences, University of Kiel, Germany. Allanite chemical analyses were performed using a JEOL Hyperprobe JXA-8500F EMPA at the Deutsches GeoForschungsZentrum in Potsdam, Germany. The data were obtained by wavelength-dispersive X-ray analysis (WDS) techniques. An accelerating voltage of 20 kV, a probe current of 40 nA (epidote) or 20 nA (allanite), and a fully focused beam were used for the analyses. The background counting times were always set to half of the respective peak counting times. Standards were natural minerals (e.g. wollastonite, corundum, forsterite, apatite, rutile) as well as synthetic materials (e.g. Sr-bearing glass, REE phosphates, U-, Th-, Ta-metals). Prior to analysis, the internal zonation of minerals was carefully checked using backscattered electron (BSE) and cathodoluminescence images. The CITZAF routine in the JEOL software, which is based on the $\Phi(\rho Z)$ method (Armstrong 1995), was used for data quantification of the raw data.

Whole rock

Four samples were sent to Activation Laboratories Ltd. in Ontario, Canada for whole-rock analysis. The samples were pulverised to fine powder with a Fritsch planetary mill using agate tools. SiO_2, Al_2O_3, Fe_2O_3 (total), MnO, MgO, CaO, Na_2O, K_2O, TiO_2, P_2O_5, Sc, Be, V, Ba, Sr, Y, and Zr were measured using the 'Lithium Metaborate/Tetraborate Fusion - ICP' method. Cr, Co, Ni, Cu, Zn, Ga, Ge, As, Rb, Nb, Mo, Ag, In, Sn, Sb, Cs, La, Ce, Pr, Nd, Sm, Eu, Gd, Tb, Dy, Ho, Er, Tm, Yb, Lu, Hf, Ta, W, Tl, Pb, Bi, Th, and U were measured using the 'Lithium Metaborate/Tetraborate Fusion—ICP/MS' method. Additionally, Cd, Cu, Ni, Zn, S (as sulphide) Ag, and Pb were measured using the 'Total Digestion - ICP' method for better quantification.

Results

Results of the analytical sessions for epidote, allanite, and whole rock are given in Online Resources 1–3, respectively. The computational data analysis for the REE was conducted using `R` (R Core Team 2014) and `ggplot2` (Wickham 2009), and is available in Online Resource 4. Raw data for X-ray mapping and `GMT` scripts (Wessel and Smith 1991) to reproduce the images are available in Online Resource 5. Full and additional X-ray maps are available in Online Resource 6.

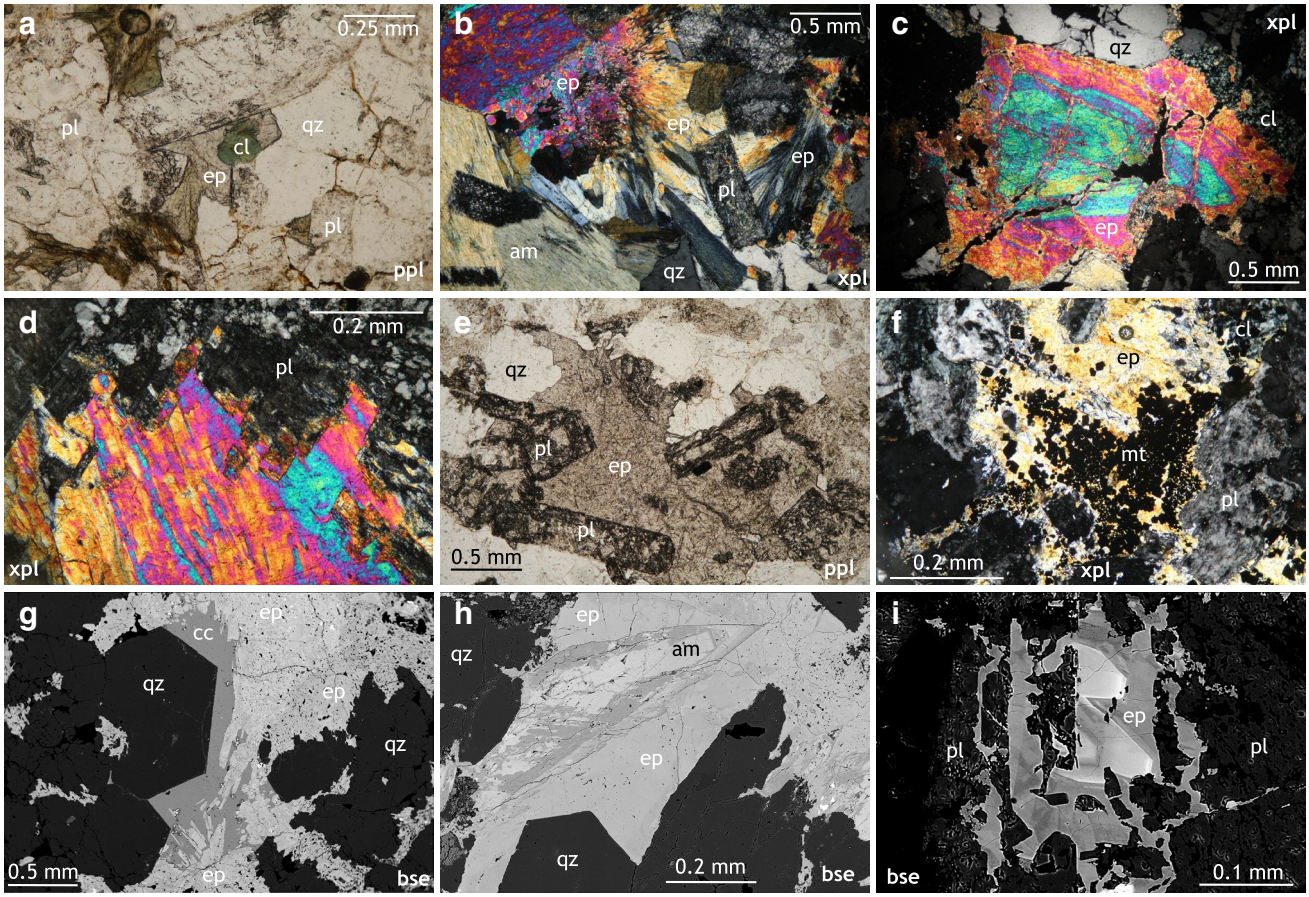

Fig. 4 'Miarolitic' epidotes. Photomicrographs: **a** PXD-1: interstitial epidote, **b** KPG-2: miarolite-containing epidote, euhedral plagioclase ghosts and amphibole, **c** SE-3E: normally zoned epidote, **d** SE-1C: euhedral plagioclase, partially altered by epidote, lining a miarolite wall filled by epidote, **e** SE-4A: euhedral quartz and ghost plagioclase lining a miarolite wall filled by epidote, and **f** SE-2A: euhedral magnetite and epidote in a miarolite. BSE images: **g** SA-1: epidote, euhedral quartz and calcite filling a miarolite, **h** KPG-2: zoned amphibole and euhedral quartz lining a miarolite filled by epidote, and **i** KPC-2X: zoned epidote filling a dissolution cavity in plagioclase

Epidote

Epidote REE patterns are given in Fig. 7. The patterns show high variability in total REE contents (hereafter referred to as $\sum$REE*, defined as the sum of all normalised REE contents, except Eu to negate any bias due to the Eu anomaly), Eu anomalies ($Eu_N/\sqrt{Sm_N \times Gd_N} = Eu_N/Eu^*$), curvature, and La_N/Lu_N ratios. A consistent feature is that epidotes with lower $\sum$REE* have stronger positive Eu anomalies. This is more apparent in Fig. 8 where linear regression models of Eu_N/Eu^* versus $\sum$REE* have been added in order to emphasise it. For every locality, most analyses plot along a band from $Eu_N/Eu^* < 1$–REE-rich analyses at the top left to $Eu_N/Eu^* > 1$–REE-poor analyses at the bottom right. The textural type of epidote ('miarolite' or 'replacement') does not seem to matter in respect to the location of the spot analysis along the line. Note, however, that in the Spilia case, the two textural types may represent two separate parallel trends. This variability in REE patterns occurs on a sample scale but also in the scale of a single grain. A remarkable example is seen in a zoned epidote from sample SE-3A, where the Eu anomaly is negative in the core of the mineral grain, but gradually becomes positive—along with REE depletion—towards the rim (Fig. 9).

Allanite

Allanite-(Y) exhibits few systematic elemental associations, i.e. zones where a group elements is consistently rich or poor relative to the rest of the grain, as qualitatively revealed in the X-ray maps. Y (proxy for heavy REE: HREE) and Ce (proxy for light REE: LREE) can be either positively or negatively associated (Fig. 10). In one grain, Ti is zoned in a unique pattern, different from the other elements and is either negatively or positively associated with the REE (Fig. 10). In a different grain, Ti is uniformly enriched in the early allanite core but not in the later allanite–epidote oscillations (not shown here, see Online

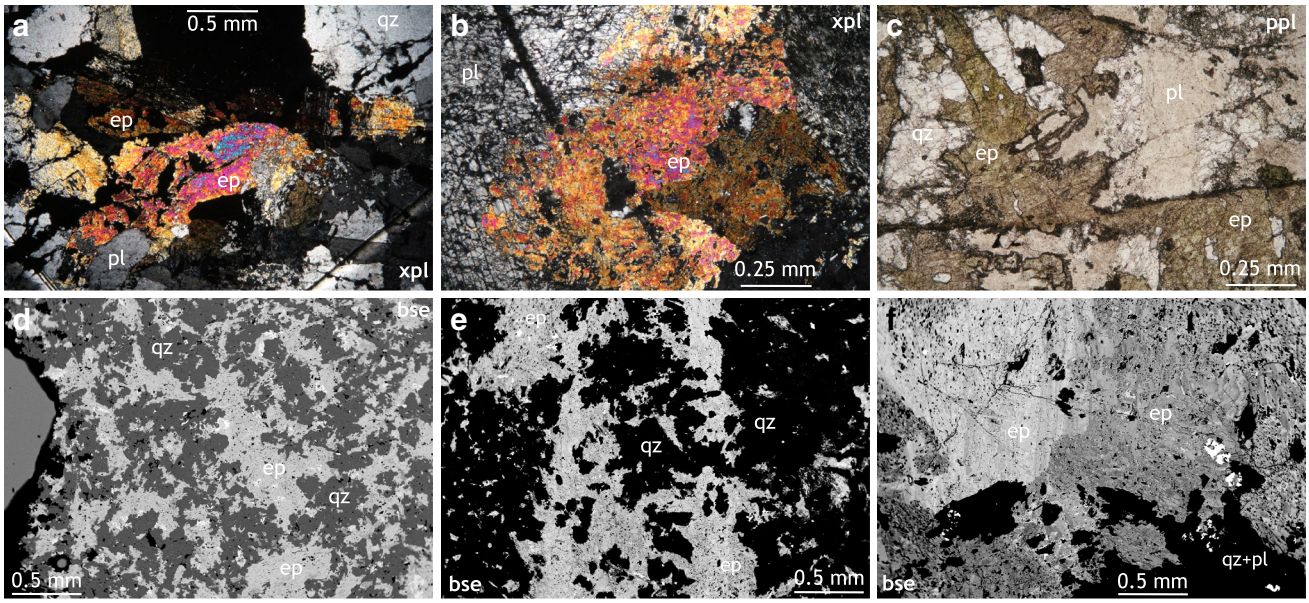

Fig. 5 'Replacement' epidotes. Photomicrographs of partly epidotised plagiogranites: **a** SX-1A, **b** KPC-4C, and **c** H-3A. BSE images: **d** Cy4-1-10: completely epidotised diabase, **e** KPX-2B: completely epidotised vertical vein in plagiogranite, and **f** SE-3A: partly epidotised plagiogranite

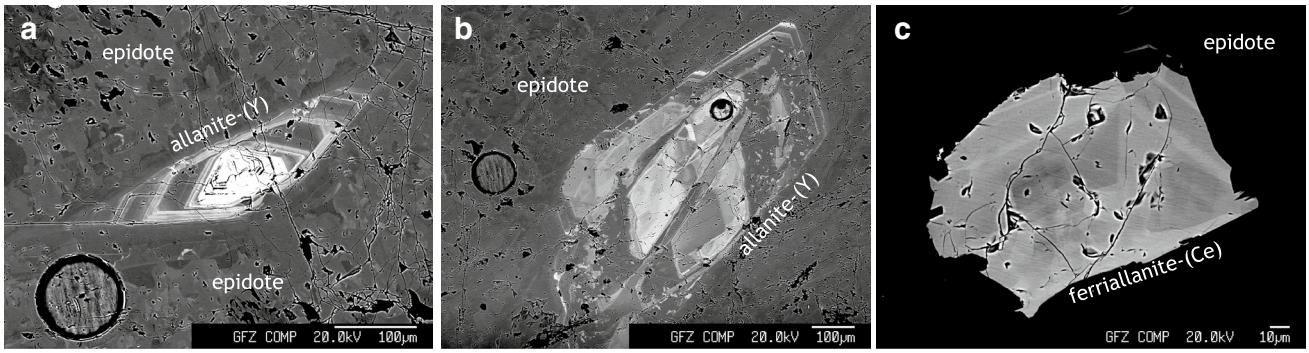

Fig. 6 BSE images of allanites: **a** SE-3A: oscillatory zoned allanite-(Y) and epidote, **b** SE-3A: oscillatory zoned allanite-(Y) and epidote, and **c** SG-1B: ferriallanite-(Ce)

Resource 6). Mn also seems to be zoned independently of other elements. Mg is the only analysed element—other than the obvious Si, Ca, Al, and Fe—that appears to have positive association with the REE. Areas abundant with REE are likewise rich in Mg, suggesting that it may have a role in the incorporation of the REE into the crystal lattice (the 'dissakisite' component; Armbruster et al. 2006).

In contrast to the lack of zoning observed in BSE images of ferriallanite-(Ce) (Fig. 6c), X-ray maps reveal that the ferriallanite-(Ce) is continuously zoned chemically from core to rim (Fig. 11). Ce and Y are negatively associated, with Ti contents usually following those of Ce. Mg is not uniformly distributed as opposed to allanite-(Y) and shows a zoning pattern mostly independent of the other elements, similarly to Mn. A single exception is a prominent thin zone near the rim of the grain that is rich in Ce, Mg, and Ti, and poor in Y and Mn.

REE plots of representative allanite analyses of sample SG-1 obtained using EMPA are given in Fig. 12. The results are most reliable for the LREE, but not as much for the HREE: Reported values for Dy seem to underestimate the true value as overall REE concentrations decrease, and vice versa for Lu (see Online Resource 4), thus the Dy value is interpolated and Lu is omitted in Fig. 12. The characteristic X-ray lines of Eu overlap with other elements and concentrations are overall very low, causing measurements of Eu contents by EMPA to be highly unreliable. Although Eu was not analysed by EMPA, it is possible to compare

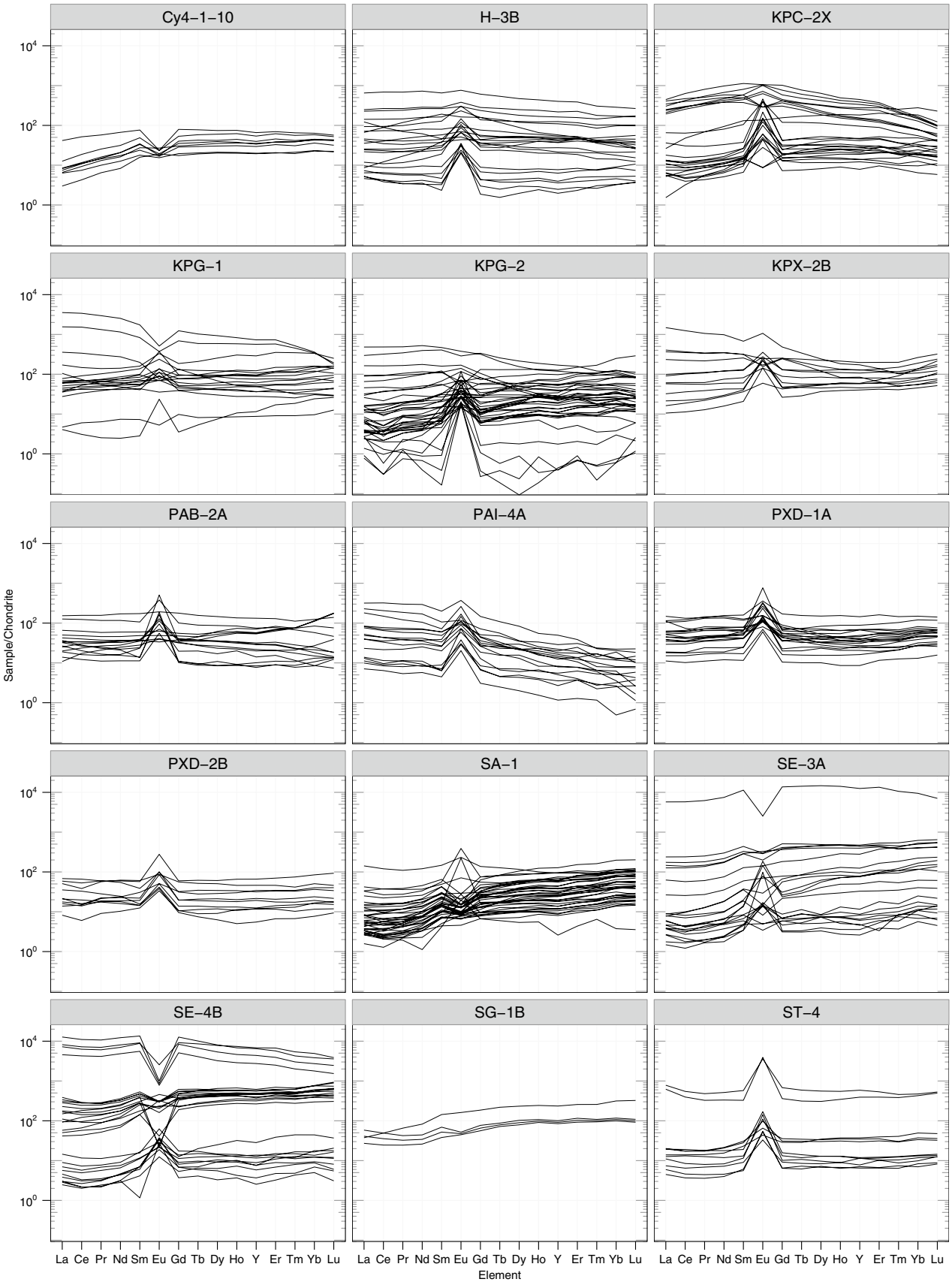

Fig. 7 REE plots of all epidote samples in this study

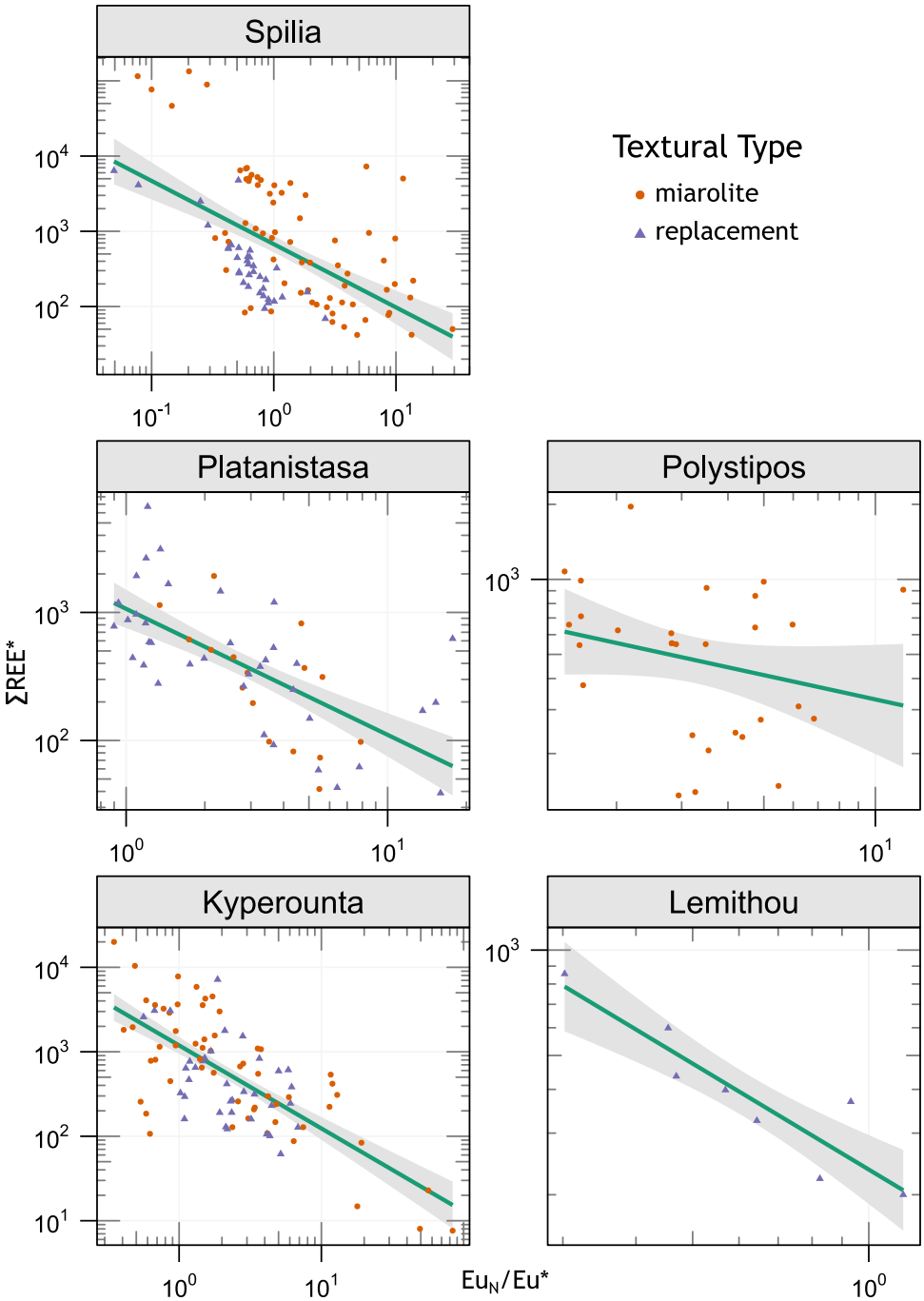

Fig. 8 Plots of ∑REE* versus Eu_N/Eu^* for the entire epidote database for each locality in logarithmic scale. *Green lines* are linear regression models with 90 % confidence intervals in *grey*

the allanites with adjacent REE-rich epidote analysed by LA-ICP-MS, which is similar to epidote from the zoned oscillations (see LA pits in Fig. 6). Such REE-rich epidote is characterised by a negative Eu anomaly (violet diamonds in Fig. 12). On this ground, negative Eu anomalies of similar magnitude can be inferred for the allanites as well.

Ferriallanite-(Ce) is strongly LREE enriched ($La_N/Yb_N \approx 30-45$), becoming less enriched with increasing atomic number. Conversely, allanite-(Y) exhibits a rather flat to weakly LREE-enriched pattern ($La_N/Yb_N \approx 1-4$), with slight enrichment of the MREE (middle REE; $La_N/Sm_N \approx 0.4-1$). Elements heavier than Sm are concentrated in allanite-(Y), whereas elements lighter than Sm are concentrated in ferriallanite-(Ce).

It is possible to estimate the redox conditions of iron in the allanites using a ∑REE+Y+Th+U versus Al diagram. A similar diagram, excluding Y and U, was described and formulated by Petrík et al. (1995) and Poitrasson (2002). In their studies, Y was a negligible component of allanite and it was safe to exclude it. However, in the present study, Y

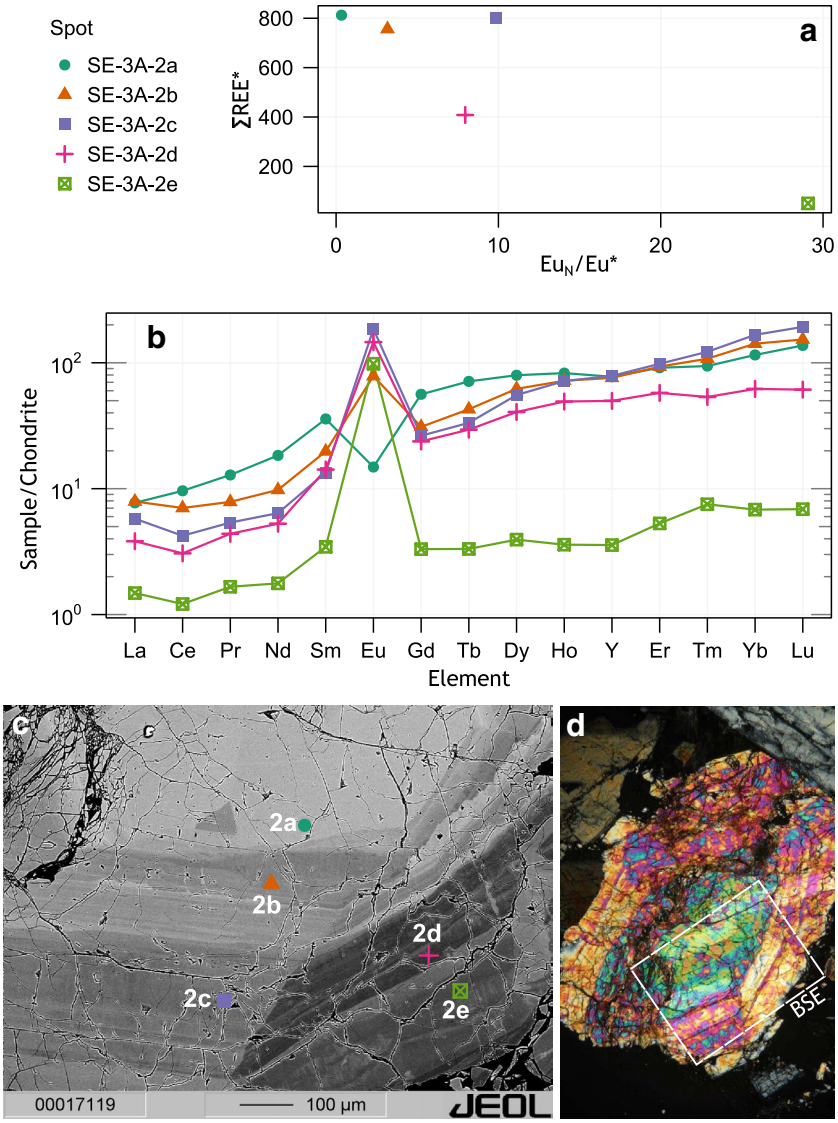

Fig. 9 REE characteristics of a zoned epidote grain from sample SE-3A. **a** $\sum$REE* versus Eu_N/Eu^* plot. **b** REE patterns. **c** BSE image with locations of analyses marked. **d** Cross polars micrograph of the epidote grain with the BSE image outline marked. An X-ray map of selected major and minor elements for this grain is available in Online Resource 6

plays a significant role and it behaves similarly to the REE, so it is included. Also, as U was analysed and it behaves similarly to Th (Frei et al. 2004), it is also included for completeness. The diagram shows four members of the epidote group: clinozoisite at the bottom right corner, epidote at the bottom left, allanite at the top right, and ferriallanite at the top left corner. Figure 13 shows that both ferriallanite-(Ce) and allanite-(Y) in sample SG-1 plot on the same Fe_{ox} line, with $Fe^{3+}/(Fe^{3+}+Fe^{2+})\approx 0.5$. The allanite-(Y) from sample SE-3 shows a trend of increasing Fe_{ox} from 0.5 to almost 1. This trend should not be interpreted in terms of changing redox conditions in the mineralising fluid, but rather as dwindling of REEs available for allanite growth, similar to allanites studied by Oberli et al. (2004). It is important to note, nonetheless, that the most REE-rich spot of the allanite-(Y) in sample SE-3, located in the core of the mineral (hence most primitive), has a Fe_{ox} value of 0.5, similar to the allanites from sample SG-1, suggesting the redox conditions at the beginning of the allanite-(Y) growth were similar to those prevailing during ferriallanite-(Ce) growth.

Whole rock

Results of whole-rock analyses for plagiogranites from Spilia are given in Fig. 14. Additional analyses of the Spilia plagiogranites given in Freund et al. (2014) are shown for comparison. The Spilia plagiogranites are REE-enriched: about 10–30 times chondrite abundance. They are LREE depleted ($La_N/Lu_N < 1$) and have a negative europium anomaly, similar to earlier measurements reported in Kay and Senechal (1976). A notable feature is the concave pattern of the LREE, which is unique to the Spilia plagiogranites according to further analyses conducted by Freund et al. (2014).

Table 2 Average concentrations and RSD of two reference basaltic glasses

BCR2G ($n = 12$)												
Element	Si	Ti	V	Cr	Co	Cu	Zn	Sr	Y	Zr	La	Ce
Measured	232960	13017	387	14	34.26	15	131	308	29.81	158	22.56	47.59
Certified		14100	425	17	38	21	125	342	35	184	24.7	53.3
RSD	4.7	2.8	1.5	6.0	1.6	1.9	5.2	1.6	1.9	1.6	1.9	1.6
Element	Pr	Nd	Sm	Eu	Gd	Tb	Dy	Ho	Er	Tm	Yb	Lu
Measured	4.82	21.99	5.62	1.95	5.27	0.80	4.63	0.89	2.21	0.30	1.96	0.27
Certified	5.35	24.5	6.1	2.07	6.16	0.92	5.28	0.98	2.56	0.34	2.01	0.279
RSD	2.7	2.8	3.9	7.0	4.3	3.7	2.6	6.1	5.4	7.4	9.7	9.5
BHVO2G ($n = 14$)												
Element	Si	Ti	V	Cr	Co	Cu	Zn	Sr	Y	Zr	La	Ce
Measured	223218	16280	306	265	42.32	106	104	367	20.83	141	13.91	34.75
Certified		16726	308	293	44	127	102	396	26	170	15.2	37.6
RSD	4.9	2.7	1.0	3.0	1.7	2.3	4.3	2.0	2.9	2.5	1.7	1.3
Element	Pr	Nd	Sm	Eu	Gd	Tb	Dy	Ho	Er	Tm	Yb	Lu
Measured	5.99	25.59	6.12	1.83	5.96	0.93	5.71	1.14	3.30	0.48	3.25	0.48
Certified	6.7	28.9	6.59	1.97	6.71	1.02	6.44	1.27	3.7	0.51	3.39	0.503
RSD	2.2	2.3	4.1	5.3	3.8	3.6	3.2	3.3	3.4	9.1	5.1	7.4

Units are in ppmw

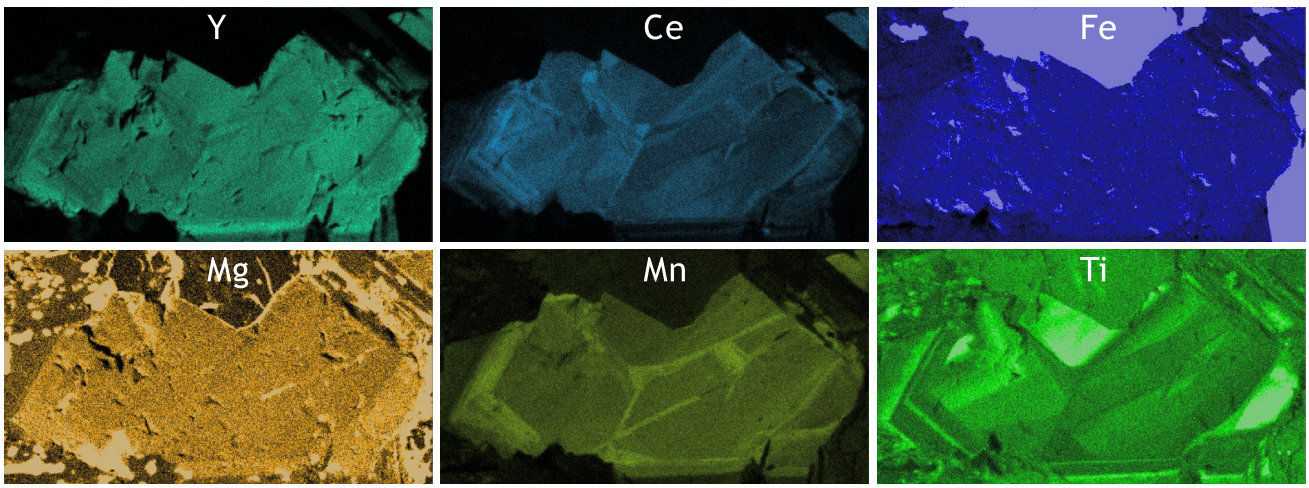

Fig. 10 X-ray map for allanite-(Y) from sample SG-1B. An X-ray map with additional elements is available in Online Resource 6

Discussion

Hydrothermal epidote

A synthesis of the petrographic evidence suggests that the allanites were the first to form, followed by the REE-rich–Eu-deficient epidotes, and lastly the REE-poor–Eu-enriched epidotes. A yet open question is at what conditions and in what medium the minerals were crystallising from. Since epidote mostly appears as vug-filling crystals, it is probably not the result of solid-state metamorphic growth in the greenschist facies, so common in the diabases of the Troodos ophiolite. It is then either of hydrothermal or magmatic origin. A magmatic origin can be easily ruled out because magmatic epidote requires high pressures that were not attained in Troodos (Schmidt and Poli 2004). A hydrothermal origin for the epidote is thus most plausible.

The negative $\sum$REE*–Eu_N/Eu^* correlation in epidote, and consequently in the fluid, may represent a continuum of two end member fluid compositions:

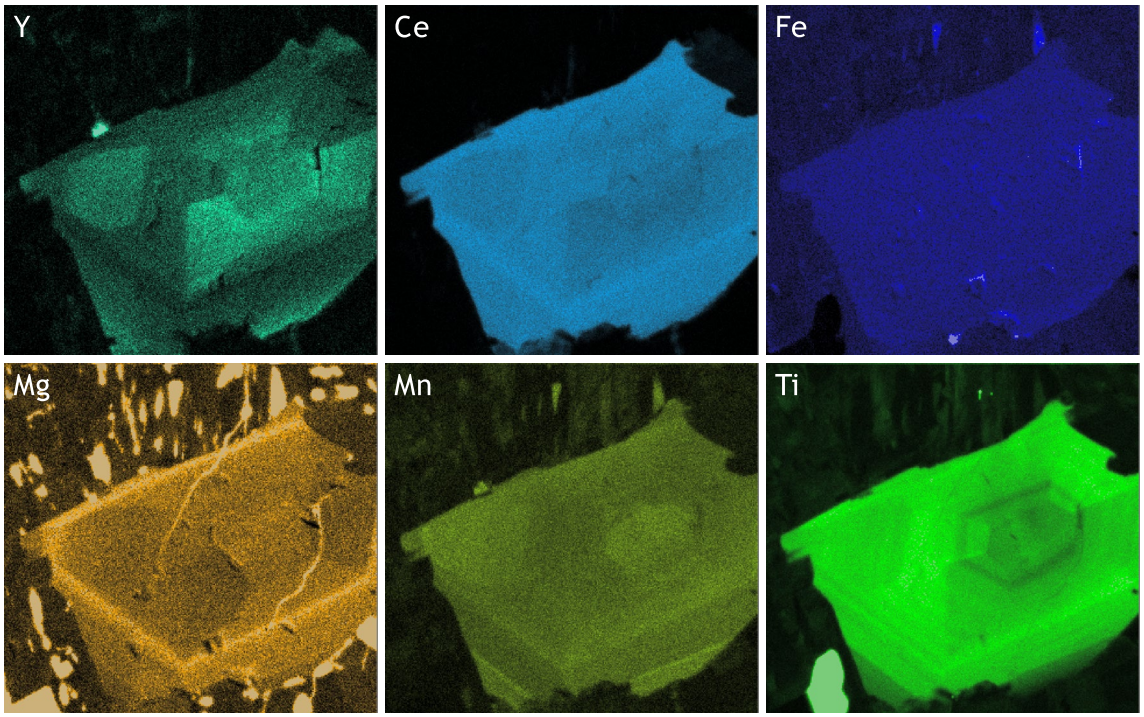

Fig. 11 X-ray map for ferriallanite-(Ce) from sample SG-1B. A BSE image of this grain is given in Fig. 6c. An X-ray map with additional elements is available in Online Resource 6

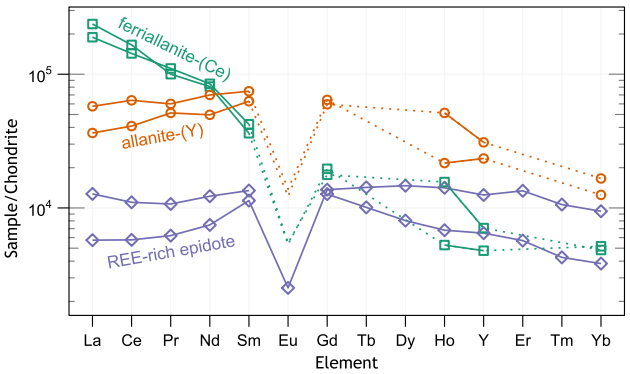

Fig. 12 REE plot for the allanites analysed in this study. Two REE-rich epidote are added for comparison: one from sample SE-4B and another from SE-3A (see Fig. 7)

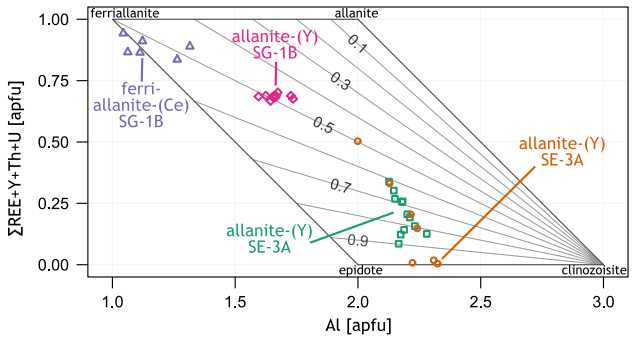

Fig. 13 Fe redox diagram for allanite, based on the method of Petrík et al. (1995). Oblique contours are $Fe_{ox} = Fe^{3+}/(Fe^{3+} + Fe^{2+})$. Allanite identification key: *violet triangle*, Fig. 11 and 6c, *pink diamond*, Fig. 10, *green square*, Fig. 6b, *orange circle*, Fig. 6a

1. The first end member is a deuteric fluid, exsolved from the crystallising plagiogranitic magmas. Epidotes of deuteric origin are not unknown (e.g. in plagiogranites described by Pedersen and Malpas 1984). Hence, the deuteric fluid inherited REE enrichment and negative europium anomaly from the highly evolved magma. Its REE characteristics are thus similar to the whole-rock composition of the plagiogranites (Fig. 14) and are best represented by REE-rich epidotes.
2. The second end member has similarities with seawater-derived hydrothermal fluid, such as fluids venting from black smokers on the sea floor (also see similar epidote grain analysed by Gillis et al. 1992 and epidosite whole-rock analysed by Valsami and Cann 1992). This fluid has a strong positive Eu anomaly and low total REE abundances, although higher than regular seawater (Michard et al. 1983; Klinkhammer et al. 1994; Craddock et al. 2010).

The $\sum$REE*–Eu_N/Eu^* trend in Troodos epidotes (Fig. 8) can be accounted for by either of two models: (1) mixing of deuteric fluid (first end member) with actual sea-

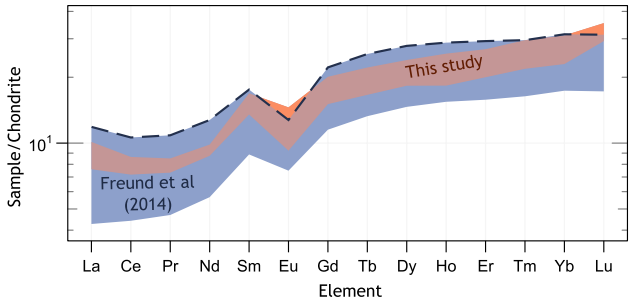

Fig. 14 REE plots for whole-rock analyses from Spilia. Orange area marks rocks from this study and violet area marks rocks from Freund et al. (2014)

water-derived fluid or (2) gradual evolution of deuteric fluid to a fluid that has similar composition to seawater-derived fluids.

There are several reasons why the mixing model is unlikely. Firstly, if modified seawater had diluted magmatic fluids to variable extents, then the same REE pattern would have been expected in all REE-poor, (modified) seawater dominated, epidotes. However, this is not the case. REE-poor epidotes in Fig. 7 show a variety of patterns, for example LREE-depleted (Cy4-1-10, KPX-2B), LREE-enriched (PAI-4A), convex (H-3B), and more. Also, the low ∑REE* analyses in Fig. 8 should converge to a single hypothetical seawater-derived fluid, but they do not. Therefore, the scatter results from local fluid variations. One may suggest that this variability in REE patterns may stem from differing conditions (pH, salinity, etc.), but Migdisov and Williams-Jones (2014) show that the REE do not significantly fractionate due to variations in fluid chemistry. Secondly, seawater could only infiltrate the plagiogranites after the transition from ductile to brittle deformation, during post-crystallisation cooling of the already solidified plagiogranite (Kelley and Delaney 1987; Gillis and Roberts 1999; Kelley and Früh-Green 2000; Gillis 2003). Thus, oscillatory zoning (Fig. 6) between deuteric patterns and actual seawater-derived fluid patterns is improbable. It is more likely that the continuous spectrum in epidote compositions is a result of gradual transformation of a deuteric-type fluid into a fluid that shares its REE pattern with seawater-derived fluids, but did not actually originate from it.

This transformation has two components: (1) reduction in REE and (2) increase in Eu. A possible explanation for lower REE contents in later epidote is decrease in temperature. Epidote in Troodos crystallised over a 100 °C range, from about 400 to 300 °C (Kelley and Robinson 1990; Petko 1997). Feineman et al. (2007) demonstrate that in the case of high-pressure zoisite (an orthorhombic member of the epidote group, with a composition similar to that of epidote, excluding Fe), REE *D* are roughly half an order of magnitude lower per 100 °C decrease in temperature. This is not sufficient to explain the larger variations in REE contents observed in the Troodos epidote (Fig. 7). As variations in temperature cannot explain the ∑REE* trend, a more likely explanation is the sequestration of REE into the crystallising epidotes, forming from fluids that become progressively depleted in ∑REE* with time. The increase in Eu can be attributed to incorporation of divalent Eu into the epidote crystal structure. Eu is highly compatible in epidote (Pan and Fleet 1996) due to the very similar ionic radius of divalent Eu compared to Sr (Valsami and Cann 1992)—by itself a highly compatible element in epidotes (Frei et al. 2004). Eu is present in sub-seafloor hydrothermal fluids in the reduced divalent state, which is highly mobile in chlorine-rich fluids (Sverjensky 1984; Bau 1991; Allen and Seyfried 2005), such as fluids exsolved during plagiogranite crystallisation. As the progressive REE-depletion of Troodos epidotes records evolution of fluid composition in time, strong positive Eu anomalies in such epidotes suggest that sufficient time has elapsed for the acidic chlorine-rich fluids to leach Eu from the country rock and make it available for incorporation into epidote in its divalent state. No major REE-hosting secondary minerals occur in association with epidote, so this trend cannot be explained by REE partitioning with competing minerals.

Hydrothermal versus magmatic allanite

A similar deuteric origin can be suggested for allanite-(Y) as well. REE-rich epidote and allanite-(Y) are oscillatory zoned (Fig. 6a, b). Since rapid oscillations between hydrothermal and magmatic conditions are doubtful, they probably share the same, contemporaneous, hydrothermal origin. This also supports the idea that the fluids are deuteric and not seawater derived, because seawater, albeit modified and enriched in REE, has not been documented crystallising allanite. In contrast, ferriallanite-(Ce) does not seem to be a part of the epidote–allanite-(Y) continuum so its origin has to be determined using different methods. Cerium-rich allanites are common minerals in many rock types and unlike epidote, do not require high pressure for magmatic crystallisation (Schmidt and Poli 2004; Gieré and Sorensen 2004). They are by far the most dominant species of the allanite group (Gieré and Sorensen 2004). Melting experiments on plagiogranite-like rocks by Nakajima and Arima (1998) show that allanite is the magmatic mineral that crystallises upon REE saturation in such rocks. However, the experimental runs were doped with REE and no analyses of the resulting allanite are given, so it is not possible to determine the exact allanite species. Conversely, allanite-(Y) is a rare mineral with very few references in the scientific literature. The coexistence of both minerals has been reported only once in granites

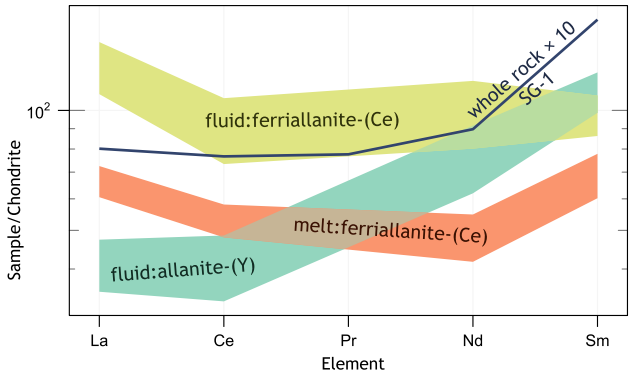

Fig. 15 Calculated LREE composition of hypothetical fluid in equilibrium with allanite-(Y) in *green* and ferriallanite-(Ce) in *yellow*, and hypothetical LREE composition of granitic melt in equilibrium with ferriallanite-(Ce) in *orange*. Both allanite compositions are from sample SG-1B. *D* values for Pr given in Banks et al. (1994) result in a spurious Pr anomaly, and *D* values are not given at all in Mahood and Hildreth (1983). Therefore, Pr values were interpolated. Whole-rock LREE contents of sample SG-1 (multiplied by 10) added for reference

of the Graciosa Province, southern Brazil, where ferriallanite-(Ce) is considered a magmatic mineral whereas allanite-(Y) crystallised from a hydrothermal fluid (Vlach and Gualda 2007; Vlach 2012). Although the granites of the Graciosa Province formed in a different tectonic setting than the Troodos ophiolite, there is a possibility that allanites in both areas formed in a similar way.

In order to test this idea, the REE patterns of the melt or fluid from which the allanites could have crystallised were calculated. *D* values for allanite/melt (Mahood and Hildreth 1983) and for allanite/fluid (Banks et al. 1994) were used to calculate the REE patterns of the fluid with which allanite-(Y) was in equilibrium, and of melt or fluid that coexisted with ferriallanite-(Ce). Unfortunately, both Mahood and Hildreth (1983) and Banks et al. (1994) provide *D* values only for the LREE. This is not a major drawback, however, since the LREE show the greatest variation among the two allanites (Fig. 12). For the calculation, two representative analyses of allanite-(Y) and ferriallanite-(Ce) from sample SG-1B were taken. Both Mahood and Hildreth (1983) and Banks et al. (1994) provide two sets of *D* values. Both sets of numbers were used per mineral, and the results are given as areas encompassing the range in Fig. 15. The whole-rock composition of sample SG-1, arbitrarily multiplied by 10 in order to fit in the plot scale, is also given in Fig. 15. An additional set of partition coefficients for magmatic allanites is provided by Brooks et al. (1981), but the resulting pattern is similar to the patterns derived from the Mahood and Hildreth (1983) data and is not shown here for simplicity. For details, see Online Resource 4.

There are several important points arising from the REE distribution calculations:

1. Primary magmatic minerals in plagiogranite sample SG-1 consist practically only of quartz, plagioclase, and magnetite—ignoring ferriallanite-(Ce) for now—none of which are major sinks for REE (e.g. Nielsen et al. 1992; Ewart and Griffin 1994). Thus, even while taking into account some amount of crystal fractionation, the REE whole-rock composition is the best approximation of SG-1 magma composition.
2. Hydrothermal fluid in equilibrium with allanite-(Y) retains the positive La–Ce deviation and the concave shape characteristic of the whole-rock LREE pattern. *D* values between melt and chlorine-rich aqueous fluids (common in the Troodos plagiogranites; Kelley and Robinson 1990; Kelley et al. 1992) are similar for all the LREE and are not likely to cause any fractionation of the LREE during exsolution (Reed et al. 2000). This observation gives support to the conclusion that the hydrothermal fluid is indeed deuteric in nature and represents direct exsolution from REE and fluid saturated magma.
3. Hydrothermal fluid in equilibrium with ferriallanite-(Ce) does not share the LREE pattern with the whole-rock composition. It is relatively enriched in La and does not show the positive Sm_N/Nd_N ratio, which is characteristic of the Spilia plagiogranites. In contrast, melt pattern in equilibrium with ferriallanite-(Ce) matches the whole-rock pattern better than the fluid pattern. Consequently, a magmatic origin is the most likely for ferriallanite-(Ce). This is in agreement with its abrupt crystal terminations against the neighbouring epidote inside miarolites, suggesting the end of silicate magma crystallisation and onset of hydrothermal fluid crystallisation.

Conditions of allanite growth

It is unclear exactly at what temperature range the allanites crystallised. Hydrothermal epidotes in plagiogranites are thought to form at 400 to 500 °C (Kelley and Robinson 1990), whereas plagiogranite melts are expected to crystallise completely at 700 to 800 °C. However, due to the volatile-rich composition of the residual melt, it is highly likely that ferriallanite-(Ce) kept on growing in undercooled melt similar to many pegmatite-hosted allanites (London and Morgan 2012) spanning at least part of the temperature range between 700 and 500 °C. Similar late magmatic–hydrothermal crystallisation in this temperature range has been documented elsewhere in gabbros of the Troodos ophiolite (Gillis 2002). The allanite-(Y)–epidote oscillations probably crystallised in the 400 to 500 °C temperature range similar to other epidotes in Troodos (Kelley and Robinson 1990). The oscillations themselves can be explained by depletion of REEs in the hydrothermal fluid

as allanite-(Y) sequesters them and subsequent replenishment by REE-rich fluids exsolving from adjacent magmas of the same large plagiogranite body at Spilia.

Further insights into the allanite growth process can be gained by considering the Fe_{ox} values for the allanites given in Fig. 13. Both ferriallanite-(Ce) and allanite-(Y) from sample SG-1 plot on the $Fe_{ox} = 0.5$ line, suggesting that both minerals crystallised from a fluid or melt having similar f_{O_2}, consistent with coexisting magnetite crystals that also occur in association with the allanites. Thus, the hydrothermal fluid inherited the oxidation state of the melt, resulting in similar Fe^{3+} to Fe^{2+} ratios. The observation that all allanites in this study share the same Fe_{ox} values suggests that the activity of available Fe^{2+} was the limiting factor for initial REE incorporation into the allanite crystal structure, and not the availability of the REE themselves. This supports the claim that ferriallanite-(Ce) crystallisation in the magmatic phase was immediately followed by allanite-(Y) crystallisation in the fluid phase. Subsequent increase in Fe_{ox} recorded in the crystal most probably records the REE depletion of the fluid (Fig. 13). Note that the increasing Fe_{ox} trend does not strictly reflect evolution in time but rather a range of oscillations in allanite-(Y)–epidote composition.

Hydrothermal fluid flow and migration

The whole-rock REE contents of the Spilia plagiogranite reported here and in Freund et al. (2014) are apparently contradictory: how can the allanite-bearing plagiogranites from this study contain less overall REE than the most REE-rich yet allanite-absent plagiogranites of Freund et al. (2014) (dashed line in Fig. 14)? Also, note that while the LREE contents in this study are lower, HREE are similar (and even higher for Lu). A possible explanation lies with the epidote/fluid D values for the REE. Unfortunately, no data are available in the literature regarding epidote, but data exist for zoisite. Two different studies have shown that partition coefficients for the REE increase with increasing atomic number, i.e. La has the lowest mineral/fluid D, whereas Lu has the highest (Brunsmann et al. 2001; Feineman et al. 2007). One can hypothesise a situation in which the REE-richest plagiogranite of Freund et al. (2014) is just on the verge of exsolving a REE-rich fluid phase. The plagiogranites of the present study show the next stage in the plagiogranite evolution: crystallisation of ferriallanite-(Ce) followed by deuteric allanite-(Y) and epidote. The epidote retains most of the HREE owing to their high partition coefficients, but the LREE are only partly incorporated to epidote and remain dissolved in the hydrothermal fluid. The LREE are then susceptible to fluid migration, which explains why they are less abundant in rocks that experienced fluid saturation. Fluid migration is indicated by the observation of similar fluid evolution pattern in epidotes in rocks other than plagiogranites. Epidotes from an epidositic diabase sampled within the sheeted dyke sequence at Lemithou (Fig. 1) exhibit the same $\sum$REE*–Eu_N/Eu^* trend characteristic of plagiogranitic epidotes (Fig. 7). Epidotisation of sheeted dykes is usually attributed to the effect of modified seawater (Richards et al. 1989; Bettison-Varga et al. 1995), but it is unlikely in this particular case due to the differing REE patterns of the epidotes from this sample. A more likely explanation is that the fluids responsible for epidote growth originated from the plutonic complex, and more specifically from a fluid saturated crystallising plagiogranite body: The sampling location is adjacent to a large plagiogranite body in the plutonic complex of the Troodos ophiolite. This plagiogranite body was not studied in this work, but Freund et al. (2014) did sample and analyse it (their 'main group'). The measured REE patterns of the 'main group' plagiogranites show striking similarities with the REE patterns of the Lemithou diabase epidote, further corroborating the fluid migration model. This process requires REE-loss associated with fluid migration from the plagiogranite outwards, which accounts for the contrasting REE patterns of allanite-bearing and allanite-lacking plagiogranites, for instance as observed in Spilia.

Autometasomatism and the textural types of epidote

The two textural types of epidote have yet to be explained in the context of the process described hithertho. It is seen by the distribution of the 'miarolite' and 'replacement' epidotes in Fig. 8 that there is little correlation between the textural type and the time of epidote crystallisation (early versus late, especially note epidotes from Kyperounta and Platanistasa). Petrographic evidence indicates that in some cases an epidote that appears to be chemically homogeneous or continuous fills in a miarolite and progresses to replace plagioclase in the miarolite walls (Fig. 4d, i). Similar phenomenon was described in the sheeted dyke sequence of Troodos by Lipfert (1997) and in Oman by Nehlig et al. (1994). Thus, epidote growth process has no preference in respect of the location within the plagiogranite. It appears that early REE-rich epidotes will grow in either miarolites, hydro-fractures, or as replacement of plagioclase, pending availability of each micro-setting. Epidote growth is in fact an opportunistic form of autometasomatism, whereby the plagiogranite is epidotised by the means of its own exsolved fluids. Growth of epidote from magmatic fluids has been suggested before based on fluid inclusion studies from Troodos (Kelley and Robinson 1990; Kelley et al. 1992; Nehlig 1991; Hayes 1996; Petko 1997), Tonga (Banerjee et al. 2000; Banerjee and Gillis 2001), and Oman (Stakes and Taylor 2003; Nicolas et al. 2008).

In contrast to Kyperounta and Platanistasa, the case of Spilia shows a different picture (Fig. 8). Here, the two

epidote types seem to form two separate parallel trends. This observation can be explained by epidotisation occurring in two stages. As shown previously, the Spilia plagiogranites contain the largest miarolites (and consequently had the largest fluid contents) and were the only plagiogranites in this study capable of crystallising allanite. It is possible that the miarolites were large enough to easily accommodate allanite and epidote growth first, before the replacement process began. An example can be seen in Fig. 2a where a rock is mostly unepidotised, yet contains epidote-filled miarolites. A second stage would require an influx of REE-bearing fluids, albeit with lower initial REE contents. Such fluids would cause epidotisation (i.e. Fig. 2c) of the plagioclase, while the pre-existing 'miarolite' epidote remains intact. The source of the second stage fluids would have to be from a similar nearby plagiogranite body.

Concluding remarks

1. The occurrence of allanite in plagiogranites must not be ignored when constructing REE models of plagiogranite formation processes. Although rare, allanite is a major carrier of REE and it should be taken into account. Furthermore, care has to be taken when establishing the crystallisation mechanism of allanite—whether magmatic or hydrothermal—in order to correctly choose the appropriate partition coefficients (*D*).
2. REE contained in exsolved hydrothermal fluids are able to migrate through the plagiogranites into themselves and into nearby rock suites. This can cause epidotisation by magmatic fluids, in contrast to the currently accepted model of epidotisation by seawater-derived hydrothermal fluids. The preferential uptake of the HREE by concurrently crystallising epidotes serves to lock the HREE in the rock while the LREE are free to move. This may result in a lower La_N/Lu_N ratio of the rock than would be in the case that REE-rich fluid had not exsolved (see Fig. 14).
3. Epidotisation of plagiogranites, in some cases, contains a significant component of autometasomatism rather than alteration by modified seawater. As epidosites are commonly thought to be an important factor of economic mineralisation in ophiolites (Richards et al. 1989; Jowitt et al. 2012), the mechanism of epidotisation in plagiogranites is of great significance and should be re-thought and revised.
4. Recently, 'silicic magma signatures' in modern seafloor hydrothermal vents were discovered by Reeves et al. (2011). It is not unlikely that these magmatic fluids were originally exsolved by crystallising plagiogranitic magmas, similar to those described in this study.

Acknowledgments This study was funded by ISF research grant 1044/09 to Yaron Katzir. Niels Jöns and Wolfgang Bach acknowledge support from the DFG-Research Centre/Excellence Cluster 'The ocean in the Earth system'. Andreas Klügel generously assisted during the LA-ICP-MS analytical sessions. We thank Chao Zhang and an anonymous reviewer for their helpful comments, and Hugh Rollinson for his review of an earlier version of the article.

References

Allen DE, Seyfried WE Jr (2005) REE controls in ultramafic hosted MOR hydrothermal systems: an experimental study at elevated temperature and pressure. Geochim Cosmochim Acta 69(3):675–683. doi:10.1016/j.gca.2004.07.016

Armbruster T, Bonazzi P, Akasaka M, Bermanec V, Chopin C, Gieré R, Heuss-Assbichler S, Liebscher A, Menchetti S, Pan Y, Pasero M (2006) Recommended nomenclature of epidote-group minerals. Eur J Mineral 18(5):551–567. doi:10.1127/0935-1221/2006/0018-0551

Armstrong JT (1995) CITZAF: a package of correction programs for the quantitative Electron Microbeam X-ray-analysis of thick polished materials, thin-films, and particles. Microbeam Anal 4(3):177–200

Banerjee NR, Gillis KM (2001) Hydrothermal alteration in a modern suprasubduction zone: the Tonga forearc crust. J Geophys Res 106(B10):21,737–21,750. doi:10.1029/2001JB000335

Banerjee NR, Gillis KM, Muehlenbachs K (2000) Discovery of epidosites in a modern oceanic setting, the Tonga forearc. Geology 28(2):151–154. doi:10.1130/0091-7613(2000)28<151:DOEIAM>2.0.CO;2

Banks DA, Yardley BWD, Campbell AR, Jarvis KE (1994) REE composition of an aqueous magmatic fluid: a fluid inclusion study from the Capitan Pluton, New Mexico, USA. Chem Geol 113:259–272. doi:10.1016/0009-2541(94)90070-1

Bau M (1991) Rare-earth element mobility during hydrothermal and metamorphic fluid-rock interaction and the significance of the oxidation state of europium. Chem Geol 93:219–230. doi:10.1016/0009-2541(91)90115-8

Bettison-Varga L, Schiffman P, Janecky DR (1995) Fluid-rock interaction in the hydrothermal upflow zone of the Solea graben, Troodos ophiolite, Cyprus. In: Schiffman P, Day HW (eds) Low-grade metamorphism of mafic rocks, vol 296, Geol Soc Am Spec Paper, pp 81–100. doi:10.1130/SPE296-p81

Borsi L, Schärer U, Gaggero L, Crispini L (1996) Age, origin and geodynamic significance of plagiogranites in lherzolites and gabbros of the Piedmont-Ligurian ocean basin. Earth Planet Sci Lett 140(1–4):227–241. doi:10.1016/0012-821X(96)00034-9

Brooks CK, Henderson P, Rønsbo JG (1981) Rare-earth partition between allanite and glass in the obsidian of Sandy Braes, Northern Ireland. Mineral Mag 44:157–160. doi:10.1180/minmag.1981.044.334.07

Brophy JG (2009) La-SiO_2 and Yb-SiO_2 systematics in mid-ocean ridge magmas: implications for the origin of oceanic plagiogranite. Contrib Miner Petrol 158(1):99–111. doi:10.1007/s00410-008-0372-3

Brophy JG, Pu X (2012) Rare earth element-SiO_2 systematics of mid-ocean ridge plagiogranites and host gabbros from the Fournier oceanic fragment, New Brunswick, Canada: a field evaluation of some model predictions. Contrib Miner Petrol 164(2):191–204. doi:10.1007/s00410-012-0732-x

Brunsmann A, Franz G, Erzinger J (2001) REE mobilization during small-scale high-pressure fluid-rock interaction and zoisite/fluid partitioning of La to Eu. Geochim Cosmochim Acta 65(4):559–570. doi:10.1016/S0016-7037(00)00544-5

Castelli D, Lombardo B (2007) The plagiogranite-FeTi-oxide gabbro association of Verne (Monviso metamorphic ophiolite, western Alps). Ofioliti 32(1):1–14. doi:10.4454/ofioliti.v32i1.343

Chutas N (1997) Rare earth element trends in basalts and plagiogranites from the Troodos Ophiolite, Cyprus. 10th Keck symposium, pp 69–72. http://www.keckgeology.org/10th-keck-symposium-volume

Constantinou G (1995) Geological map of Cyprus. Geological Survrey Department, Cyprus

Craddock PR, Bach W, Seewald JS, Rouxel OJ, Reeves E, Tivey MK (2010) Rare earth element abundances in hydrothermal fluids from the Manus Basin, Papua New Guinea: indicators of sub-seafloor hydrothermal processes in back-arc basins. Geochim Cosmochim Acta 74(19):5494–5513. doi:10.1016/j.gca.2010.07.003

Dilek Y, Thy P (2006) Age and petrogenesis of plagiogranite intrusions in the Ankara mélange, central Turkey. Isl Arc 15(1):44–57. doi:10.1111/j.1440-1738.2006.00522.x

Ewart A, Griffin WL (1994) Application of proton-microprobe data to trace-element partitioning in volcanic rocks. Chem Geol 117(1–4):251–284. doi:10.1016/0009-2541(94)90131-7

Feineman MD, Ryerson FJ, DePaolo DJ, Plank T (2007) Zoisite-aqueous fluid trace element partitioning with implications for subduction zone fluid composition. Chem Geol 239(3–4):250–265. doi:10.1016/j.chemgeo.2007.01.008

Flagler PA, Spray JG (1991) Generation of plagiogranite by amphibolite anatexis in oceanic shear zones. Geology 19(1):70–73. doi:10.1130/0091-7613(1991)019<0070:GOPBAA>2.3.CO;2

Flawn PT (1951) Nomenclature of epidote rocks. Am J Sci 249(10):769–777. doi:10.2475/ajs.249.10.769

Floyd PA, Yaliniz MK, Goncuoglu MC (1998) Geochemistry and petrogenesis of intrusive and extrusive ophiolitic plagiogranites, Central Anatolian Crystalline Complex, Turkey. Lithos 42(3–4):225–241. doi:10.1016/S0024-4937(97)00044-3

France L, Koepke J, Ildefonse B, Cichy SB, Deschamps F (2010) Hydrous partial melting in the sheeted dike complex at fast spreading ridges: experimental and natural observations. Contrib Miner Petrol 160(5):683–704. doi:10.1007/s00410-010-0502-6

Frei D, Liebscher A, Franz G, Dulski P (2004) Trace element geochemistry of epidote minerals. Rev Mineral Geochem 56(1):553–605. doi:10.2138/gsrmg.56.1.553

Freund S, Haase KM, Keith M, Beier C, Garbe-Schönberg D (2014) Constraints on the formation of geochemically variable plagiogranite intrusions in the Troodos Ophiolite, Cyprus. Contrib Miner Petrol 167(2):1–22. doi:10.1007/s00410-014-0978-6

Gerlach DC, Leeman WP, Avé Lallemant HG (1981) Petrology and geochemistry of plagiogranite in the Canyon Mountain Ophiolite, Oregon. Contrib Miner Petrol 77(1):82–92. doi:10.1007/BF01161505

Gieré R, Sorensen SS (2004) Allanite and other REE-rich epidote-group minerals. Rev Mineral Geochem 56(1):431–493. doi:10.2138/gsrmg.56.1.431

Gillis KM (2002) The rootzone of an ancient hydrothermal system exposed in the Troodos ophiolite, Cyprus. J Geol 110(1):57–74. doi:10.1086/324205

Gillis KM (2003) Subseafloor geology of hydrothermal root zones at oceanic spreading centers. In: Halbach PE, Tunnicliffe V, Hein JR (eds) Energy and mass transfer in marine hydrothermal systems. Dahlem University Press, Berlin, pp 55–71

Gillis KM, Roberts MD (1999) Cracking at the magma-hydrothermal transition: evidence from the Troodos Ophiolite, Cyprus. Earth Planet Sci Lett 169(3–4):227–244. doi:10.1016/S0012-821X(99)00087-4

Gillis KM, Ludden JN, Smith AD (1992) Mobilization of REE during crustal aging in the Troodos Ophiolite, Cyprus. Chem Geol 98(1–2):71–86. doi:10.1016/0009-2541(92)90091-I

Grimes CB, Ushikubo T, John BE, Valley JW (2011) Uniformly mantle-like $\delta^{18}O$ in zircons from oceanic plagiogranites and gabbros. Contrib Miner Petrol 161(1):13–33. doi:10.1007/s00410-010-0519-x

Hayes SK (1996) Epidotization of the sheeted dike-plutonic contact, Troodos Ophiolite, Cyprus. 9th Keck symposium, pp 221–224, http://www.keckgeology.org/9th-keck-symposium-volume

Jochum KP, Willbold M, Raczek I, Stoll B, Herwig K (2005) Chemical characterisation of the USGS reference glasses GSA-1G, GSC-1G, GSD-1G, GSE-1G, BCR-2G, BHVO-2G and BIR-1G using EPMA, ID-TIMS. ID-ICP-MS and LA-ICP-MS. Geostand Geoanal Res 29(3):285–302. doi:10.1111/j.1751-908X.2005.tb00901.x

Jochum KP, Weis U, Stoll B, Kuzmin D, Yang Q, Raczek I, Jacob DE, Stracke A, Birbaum K, Frick DA, Günther D, Enzweiler J (2011) Determination of reference values for NIST SRM 610–617 glasses following ISO guidelines. Geostand Geoanal Res 35(4):397–429. doi:10.1111/j.1751-908X.2011.00120.x

Jowitt SM, Jenkin GR, Coogan LA, Naden J (2012) Quantifying the release of base metals from source rocks for volcanogenic massive sulfide deposits: effects of protolith composition and alteration mineralogy. J Geochem Explor 118:47–59. doi:10.1016/j.gexplo.2012.04.005

Kaur G, Mehta PK (2005) The Gothara plagiogranite: evidence for oceanic magmatism in a non-ophiolitic association, North Khetri Copper Belt, Rajasthan, India? J Asian Earth Sci 25(5):805–819. doi:10.1016/j.jseaes.2004.08.003

Kay RW, Senechal RG (1976) The rare earth geochemistry of the Troodos Ophiolite complex. J Geophys Res 81(5):964–970. doi:10.1029/JB081i005p00964

Kelley DS, Delaney JR (1987) Two-phase separation and fracturing in mid-ocean ridge gabbros at temperatures greater than 700 ° C. Earth Planet Sci Lett 83(1–4):53–66. doi:10.1016/0012-821X(87)90050-1

Kelley DS, Früh-Green GL (2000) Volatiles in mid-ocean ridge environments. In: Dilek Y (ed) Ophiolites and oceanic crust: new insights from field studies and the Ocean Drilling Program, vol 349, Geol Soc Am Spec Paper, pp 237–260, doi:10.1130/0-8137-2349-3.237

Kelley DS, Robinson PT (1990) Development of a brine-dominated hydrothermal system at temperatures of $400-500\,^{\circ}C$ in the upper level plutonic sequence, Troodos ophiolite, Cyprus. Geochim Cosmochim Acta 54(3):653–661. doi:10.1016/0016-7037(90)90361-N

Kelley DS, Robinson PT, Malpas JG (1992) Processes of brine generation and circulation in the oceanic crust: fluid inclusion evidence from the Troodos Ophiolite, Cyprus. J Geophys Res 97(B6):9307–9322. doi:10.1029/92JB00520

Klinkhammer GP, Elderfield H, Edmond JM, Mitra A (1994) Geochemical implications of rare earth element patterns in hydrothermal fluids from mid-ocean ridges. Geochim Cosmochim Acta 58(23):5105–5113. doi:10.1016/0016-7037(94)90297-6

Koepke J, Seidel E (2004) Hornblendites within ophiolites of Crete, Greece: evidence for amphibole-rich cumulates derived from an iron-rich tholeiitic melt. Ofioliti 29(2):159–175. doi:10.4454/ofioliti.v29i2.212

Koepke J, Feig ST, Snow J, Freise M (2004) Petrogenesis of oceanic plagiogranites by partial melting of gabbros: an experimental study. Contrib Miner Petrol 146(4):414–432. doi:10.1007/s00410-003-0511-9

Koepke J, Berndt J, Feig ST, Holtz F (2007) The formation of SiO_2-rich melts within the deep oceanic crust by hydrous partial melting of gabbros. Contrib Miner Petrol 153(1):67–84. doi:10.1007/s00410-006-0135-y

Lipfert G (1997) Epidote nodules in the sheeted intrusive complex of the Troodos Ophiolite, Cyprus. 10th Keck symposium, pp 73–76. http://www.keckgeology.org/10th-keck-symposium-volume

London D, Morgan GB (2012) The pegmatite puzzle. Elements 8(4):263–268. doi:10.2113/gselements.8.4.263

Luchitskaya MV, Morozov OL, Palandzhyan SA (2005) Plagiogranite magmatism in the Mesozoic island-arc structure of the Pekulney Ridge, Chukotka Peninsula, NE, Russia. Lithos 79(1–2):251–269. doi:10.1016/j.lithos.2004.04.056

Mahood G, Hildreth W (1983) Large partition coefficients for trace elements in high-silica rhyolites. Geochim Cosmochim Acta 47(1):11–30. doi:10.1016/0016-7037(83)90087-X

Malpas J (1987) Geological map of the Amiandos-Palekhori area 1:10,000. Geological Survrey Department, Cyprus

Mason R (1981) A trondhjemite vein in the Sulitjelma Gabbro, Norway, and its implications for the age of the Sulitjelma Ophiolite. Geol Mag 118(5):525–531. doi:10.1017/S001675680003288X

Michard A, Albarède F, Michard G, Minster JF, Charlou JL (1983) Rare-earth elements and uranium in high-temperature solutions from East Pacific Rise hydrothermal vent field (13° N). Nature 303(5920):795–797. doi:10.1038/303795a0

Migdisov AA, Williams-Jones AE (2014) Hydrothermal transport and deposition of the rare earth elements by fluorine-bearing aqueous liquids. Miner Deposita 49(8):987–997. doi:10.1007/s00126-014-0554-z

Montanini A, Travaglioli M, Serri G, Dostal J, Ricci CA (2006) Petrology of gabbroic to plagiogranitic rocks from southern Tuscany (Italy): evidence for magmatic differentiation in an ophiolitic sequence. Ofioliti 31(2):55–69. doi:10.4454/ofioliti.v31i2.329

Nakajima K, Arima M (1998) Melting experiments on hydrous low-K tholeiite: implications for the genesis of tonalitic crust in the Izu-Bonin–Mariana arc. Isl Arc 7(3):359–373. doi:10.1111/j.1440-1738.1998.00195.x

Nakamura K, Morishita T, Chang Q, Neo N, Kumagai H (2007) Discovery of lanthanide tetrad effect in an oceanic plagiogranite from an Ocean Core Complex at the Central Indian Ridge 25° S. Geochem J 41:135–140. doi:10.2343/geochemj.41.135

Nehlig P (1991) Salinity of oceanic hydrothermal fluids: a fluid inclusion study. Earth Planet Sci Lett 102(3–4):310–325. doi:10.1016/0012-821X(91)90026-E

Nehlig P, Juteau T, Bendel V, Cotten J (1994) The root zones of oceanic hydrothermal systems: constraints from the Samail ophiolite (Oman). J Geophys Res 99(B3):4703–4713. doi:10.1029/93JB02663

Nicolas A, Boudier F, Koepke J, France L, Ildefonse B, Mevel C (2008) Root zone of the sheeted dike complex in the Oman ophiolite. Geochem Geophys Geosyst 9(5):1–29. doi:10.1029/2007GC001918

Nielsen RL, Gallahan WE, Newberger F (1992) Experimentally determined mineral-melt partition coefficients for Sc, Y and REE for olivine, orthopyroxene, pigeonite, magnetite and ilmenite. Contrib Miner Petrol 110(4):488–499. doi:10.1007/BF00344083

Oberli F, Meier M, Berger A, Rosenberg CL, Gieré R (2004) U-Th-Pb and $^{230}Th/^{238}U$ disequilibrium isotope systematics: precise accessory mineral chronology and melt evolution tracing in the Alpine Bergell intrusion. Geochim Cosmochim Acta 68(11):2543–2560. doi:10.1016/j.gca.2003.10.017

Pan Y, Fleet ME (1996) Intrinsic and external controls on the incorporation of rare-earth elements in calc-silicate minerals. Can Mineral 34(1):147–159. http://canmin.geoscienceworld.org/content/34/1/147.short

Pedersen RB, Malpas J (1984) The origin of oceanic plagiogranites from the Karmoy ophiolite, Western Norway. Contrib Miner Petrol 88(1–2):36–52. doi:10.1007/BF00371410

Petko CE (1997) Epidotizing fluid temperature and composition at the sheeted dike-plutonic contact, Troodos ophiolite, Cyprus. 10th Keck symposium, pp 77–80. http://www.keckgeology.org/10th-keck-symposium-volume

Petrík I, Broska I, Lipka J, Siman P (1995) Granitoid allanite-(Ce): substitution relations, redox conditions and REE distributions (on an example of I-type granitoids, Western Carpathians, Slovakia). Geol Carpath 46(2):79–94, http://www.geologicacarpathica.com/browse-journal/archive-1950-1996/46-2/

Pin C, Paquette JL, Ábalos B, Santos FJ (2006) Composite origin of an early Variscan transported suture: ophiolitic units of the Morais Nappe Complex (north Portugal). Tectonics 25(5):TC5001. doi:10.1029/2006TC001971

Poitrasson F (2002) In situ investigations of allanite hydrothermal alteration: examples from calc-alkaline and anorogenic granites of Corsica (southeast France). Contrib Miner Petrol 142(4):485–500. doi:10.1007/s004100100303

R Core Team (2014) R: A language and environment for statistical computing. R Foundation for Statistical Computing, Vienna, Austria. http://www.R-project.org/

Reed MJ, Candela PA, Piccoli PM (2000) The distribution of rare earth elements between monzogranitic melt and the aqueous volatile phase in experimental investigations at 800 °C and 200 MPa. Contrib Miner Petrol 140(2):251–262. doi:10.1007/s004100000182

Reeves EP, Seewald JS, Saccocia P, Bach W, Craddock PR, Shanks WC, Sylva SP, Walsh E, Pichler T, Rosner M (2011) Geochemistry of hydrothermal fluids from the PACMANUS, Northeast Pual and Vienna Woods hydrothermal fields, Manus Basin,Papua New Guinea. Geochim Cosmochim Acta 75(4):1088–1123. doi:10.1016/j.gca.2010.11.008

Richards HG, Cann JR, Jensenius J (1989) Mineralogical zonation and metasomatism of the alteration pipes of Cyprus sulfide deposits. Econ Geol 84(1):91–115. doi:10.2113/gsecongeo.84.1.91

Rollinson H (2009) New models for the genesis of plagiogranites in the Oman ophiolite. Lithos 112(3–4):603–614. doi:10.1016/j.lithos.2009.06.006

Rollinson H (2014) Plagiogranites from the mantle section of the Oman Ophiolite: models for early crustal evolution. In: Rollinson HR, Searle MP, Abbasi IA, Al-Lazki AI, Al Kindi MH (eds) Tectonic Evolution of the Oman Mountains, vol 392, Geol Soc Lond Spec Pub, pp 247–261, doi:10.1144/SP392.13

Rudnev SN, Babin GA, Vladimirov AG, Kruk NN, Shokal'sky SP, Borisov SM, Travin AV, Levchenkov OA, Terleev AA, Kuibida ML (2005) Geologic setting, age, and geochemical model of the formation of West Sayan plagiogranitoids. Russ Geol Geophys 46(2):170–187

Schmidt MW, Poli S (2004) Magmatic epidote. Rev Mineral Geochem 56(1):399–430. doi:10.2138/gsrmg.56.1.399

Silantyev SA, Aranovich LY, Bortnikov NS (2010) Oceanic plagiogranites as a result of interaction between magmatic and hydrothermal systems in the slow-spreading mid-ocean ridges. Petrology 18(4):369–383. doi:10.1134/S0869591110040041

Stakes DS, Taylor HP Jr (2003) Oxygen isotope and chemical studies on the origin of large plagiogranite bodies in northern Oman, and their relationship to the overlying massive sulphide deposits. In: Dilek Y, Robinson RT (eds) Ophiolites in Earth History, vol 218, Geol Soc Lon Spec Pub, pp 315–351, doi: 10.1144/GSL.SP.2003.218.01.17

Sverjensky DA (1984) Europium redox equilibria in aqueous solution. Earth Planet Sci Lett 67(1):70–78. doi:10.1016/0012-821X(84)90039-6

Twining K (1996) Origin of plagiogranite in the Troodos ophiolite, Cyprus. 9th Keck symposium pp 245–248. http://www.keckgeology.org/9th-keck-symposium-volume

Valsami E, Cann JR (1992) Mobility of rare earth elements in zones of intense hydrothermal alteration in the Pindos ophiolite, Greece. In: Parson LM, Murton BJ, Browning P (eds) Ophiolites and their Modern Oceanic Analogues, vol 60, Geol Soc Lon Spec Pub, pp 219–232. doi:10.1144/GSL.SP.1992.060.01.13

Vlach SRF (2012) Micro-structural and compositional variations of hydrothermal epidote-group minerals from a peralkaline granite, Corupá Pluton, Graciosa Province, South Brazil, and their petrological implications. An Acad Bras Ciênc 84:407–426. doi:10.1590/S0001-37652012005000024

Vlach SRF, Gualda GA (2007) Allanite and chevkinite in A-type granites and syenites of the Graciosa Province, Southern Brazil. Lithos 97(1–2):98–121. doi:10.1016/j.lithos.2006.12.003

Wessel P, Smith WHF (1991) Free software helps map and display data. EOS Trans Am Geophys Union 72(41):441–446. doi:10.1029/90EO00319

Wickham H (2009) ggplot2: elegant graphics for data analysis. Springer, New York. doi:10.1007/978-0-387-98141-3

Wilson RAM (1959) The geology of the Xeros-Troodos area, Geol Surv Cyprus Mem, vol 1